



Mechanical properties and deformation behavior of equiatomic CoCrFeMnNi high-entropy alloy foam: A molecular dynamics study

Ezekiel Edward Nettey-Oppong^{a,*}, Emmanuel Essel Mensah^b, Elijah Effah^c, Eric Asare^c, Martinson Addo Nartey^c

^a Department of Biomedical Engineering, Yonsei University, Wonju, South Korea

^b Department of Materials Science and Engineering, Egypt-Japan University of Science and Technology, Alexandria, Egypt

^c Department of Materials Engineering, Kwame Nkrumah University of Science and Technology, Kumasi, Ghana



ARTICLE INFO

communicated by: Prof. Francois Peeters

Keywords:

High entropy alloys
Syntactic foams
Metal foams
Molecular dynamics

ABSTRACT

In recent years, the aerospace and mechanical industries have employed metal foams for High Energy Capacity applications. However, the porous nature of such metallic foams results in a drop in tensile properties. High Entropy Alloys (HEAs) have been reported to overcome the strength-ductility trade-off as opposed to conventional metals and their alloys. Based on this, an equiatomic nano porous CoCrFeMnNi HEA is investigated using molecular dynamics simulation to elucidate the deformation behavior and mechanical performance at different atom distributions, percent porosity, and pore locations. The findings indicated that the mechanical properties are independent of atom distributions. However, with an increase in percent porosity, a decline in the ultimate tensile strength was observed. Up to 66% reduction in tensile strength was recorded. A similar trend was observed under temperature variations. By varying pore location, either within or on the structure, the pores within the foam structure led to a significant reduction in properties. The deformation mechanism of the HEA foam was established via analyses of the dislocation distributions, stacking faults, crack nucleation, and propagation. The findings offer new insights for material design to produce high-performance HEA foams and a comprehension of its failure mechanism under loading.

1. Introduction

Materials with excellent mechanical properties and good Energy Absorption Capacity (EAC) are highly desired in many industries for impact protection, particularly aerospace and automobile industries [1–3]. Metal foams demonstrate high potential for energy-absorption applications due to their extended stress plateau and other distinctive physical properties including lightweight [4–8]. Even though metal foams have high EAC, the porous structure degrades other mechanical properties, particularly the ultimate tensile strength. Metal matrix syntactic foams (MMSFs) are a class of materials that exhibit high performance in energy absorption and lightweight structural applications [8]. However, the use of conventional syntactic foams (SF) such as Mg alloy SF [9,10], Al alloy SF [11,12], Zn alloy SF [13,14], steel SF [15], NiTi shape-memory alloy SF [16], and bulk metallic glass SF [17] are limited by their relatively low tensile strength. Thus, it is imperative to enhance the mechanical properties of metal foams to increase the range of applications or find alternative materials with similar or improved

properties.

Over the past decade, High-entropy alloys (HEAs) has shown a significant capability to overcome the strength-ductility trade-off as compared to conventional alloys [18–23]. HEAs are metallic materials with five or more primary elements that crystallize as a single phase with noticeably high entropy due to the equal or near-equal mixture and are usually characterized by distinct atomic structures which facilitate the interaction of multiple microscopic mechanisms [24–26]. Subsequently, HEAs possess excellent macroscopic mechanical properties including high tensile strength and hardness, high-temperature oxidation resistance, and outstanding corrosion resistance, as compared to conventional metals [25,27,28]. As such, HEAs are employed in making exhaust nozzles and gas turbine cases within the gas turbine engine [29] and for nuclear reactor applications [30]. Due to the benefits HEAs offer, HEA foams may be considered as the right alternative to overcome the shortcomings of conventional metallic foams.

Meng et al. [8] recently fabricated a novel high entropy alloy syntactic foam with CoCrFeMnNi by a gas pressure infiltration method. The

* Corresponding author.

E-mail address: ezekeiedward@yonsei.ac.kr (E.E. Nettey-Oppong).

reported HEA foam exhibited a high strength of 241.5 ± 20.3 MPa and an ultra-high energy absorption capacity (EAC) of 242.8 ± 20.6 MJm $^{-3}$, distinguishing it from conventional metal foams. However, like all metal foams, the induced porosity led to a reduction in mechanical strength. Also, Otto et al. [31] investigated the tensile properties' dependence on temperature and grain size of an equiatomic CoCrFeMnNi HEA within the temperature range of 77 K–1073 K. The work showed that yield strength, ultimate tensile strength, and elongation to fracture all increased with decreasing temperature. The fine-grain material had a superior yield strength between 77 K and 873 K, with the medium and coarse-grain materials showing a less significant yield strength, about a third of the fine-grain. However, at elevated temperatures (873 K - 1073 K), the fine grain material had a 50% decrease in yield strength, while the medium grain and coarse grain materials showed no significant decrease in yield.

Molecular Dynamics (MD) simulation is an effective complimentary tool for experimental methods which has been employed in the studies of several HEAs and metal foams to elucidate on their mechanical behavior and properties [8,32–37]. Using MD simulations, Sun et al. [38] demonstrated the superior mechanical properties of CoCrFeNi through the formation of high temperature strengthening phases after including Ti and Al to form CoCrFeNi(Al_{0.3}Ti_{0.2})_x HEA. Li et al. [39] studied the deformation behavior of Co₂₅Ni₂₅Fe₂₅Al_{7.5}Cu_{17.5} HEA and showed that at elevated temperatures and low strain rates, grain boundary sliding largely controls the plastic behavior, as opposed to dislocation slip at high strain rates and lower temperatures. Also, Sharma and Balasubramanian [35] described the interatomic interactions of the alloying elements of Al_{0.1}CoCrFeNi HEA. The dislocation mechanism after subjecting the HEA to strain was characterized by twinning and stacking faults as the dislocations nucleated.

Herein, molecular dynamics simulation is employed to extensively investigate the mechanical behavior of CoCrFeMnNi high entropy alloy foams. The effect of atomic distribution, percent porosity, and temperature on the mechanical properties of the HEA foam, as well as the deformation behavior are investigated. The deformation mechanism of the HEA foam structure under these variables is probed via analyses of the dislocation distributions, stacking faults, crack nucleation, and propagation. Additionally, the potential of MD simulations in developing HEA foam structures that circumvent the significant decline in mechanical strength is explored.

2. Computational method

2.1. HEA modeling

Molecular dynamics simulation was conducted with the Large-scale Atomic/Molecular Massively Parallel Simulator (LAMMPS) [40]. An equimolar face-centered cubic (FCC) CoCrFeMnNi HEA with three different atom distributions was simulated. The modeled quinary monocrystalline HEA structure had 21,600 atoms of each constituent element, totaling 108,000 atoms, and a simulation cell with a cubic length of 108 Å. All molecular dynamics simulations were carried out under periodic boundary conditions. The varying atom distributions were generated using the FCC lattice sites for random atom positioning of the alloying atoms. The three modeled atom distributions of the CoCrFeMnNi HEA are denoted S_a, S_b, and S_c. Different random seeds were used for each model, to generate varying individual atom coordinates, resulting in a structure with the same mole ratio but different atom distribution. The three distributions were simulated to probe the influence of atomic arrangement on the mechanical properties of the CoCrFeMnNi HEA.

2.2. Simulation details

The recently developed pair potential by Gröger et al. [41] for random FCC CoCrFeMnNi alloys was used for the interatomic potentials

in this work. To evaluate the feasibility of the pair potentials in describing the interatomic interaction of the modeled systems at different temperatures, a liquid-to-solid state quench simulation was carried out. The quench simulation was conducted under an isothermal-isobaric (NPT) ensemble. Model S_a was heated to 1200 K at 0 bar pressure for 400 ps and quenched to 70 K with a time step of 0.005 ps at a cooling rate of 0.05 K/ps. Fig. 1 shows the common neighbor analysis (CNA) of the final structure after quenching. It can be observed from the CNA that all the atoms retained their FCC configuration. The 100% FCC atom arrangement after the quench simulation confirms the capability of the chosen interatomic potential to accurately model the CoCrFeMnNi HEA system.

The steepest descent algorithm was used for the energy minimization of the simulated HEA structures, followed by an equilibration under NPT ensemble. Equilibration of the modeled systems was done at a pressure of 0 bar and temperatures of 77 K, 300 K, 650 K, and 1000 K. Furthermore, the Velocity-Verlet scheme was used to integrate Newton's equation of motion, at a time step of 0.005 ps for the equilibration dynamics. The non-Hamiltonian equations of motion was time-integrated to produce sampled velocities and positions from the isothermal-isobaric ensemble. A Nose-Hoover barostat was used to keep the pressure constant.

For the construction of the HEA foam structure, pores were generated in each of the models. It is necessary to maintain the same pore sites for all the modeled CoCrFeMnNi HEA systems to comparatively assess the effect of atomic distribution, temperature, and porosity on the mechanical properties. Subsequently, porosity was achieved in the modeled structures by designing a template with random spheres. The template design involved the construction of a 3D model of the simulation cell and the random insertion of spheres. The coordinates of each sphere derived from the template specify the pore locations in the foam structure. Furthermore, the pore volumes were attenuated via numerical methods to achieve the desired percent porosity. These derived quantities were utilized in modifying the initial HEA structures to model foam structures of specific percent porosities and consistent pore locations. The nano porous CoCrFeMnNi HEA structure was modeled by generating ten spherical pores at random locations within and at the surface of the simulation cell, as shown in Fig. 2.

The location of the spheres from the template was adopted as a spatial filter to generate voids in the HEA structures, thus, the coordinate of each pore was based on the reference template. The geometry of the pores was informed by the regular spherical pores realized in the experimental fabrication of the HEA foam [8]. This technique ensures consistency in pore geometry and volume fraction of voids for the modeled HEA systems, S_a, S_b, and S_c. The conventional technique for

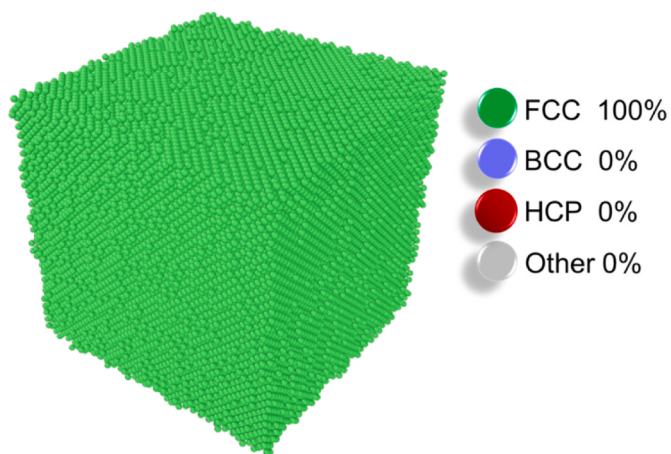


Fig. 1. Efficiency of the interatomic potential for molecular dynamics simulation of CoCrFeMnNi HEA. Common neighbor analysis (CNA) of the resulting structure after quench simulation, from 1200 K to 70 K.

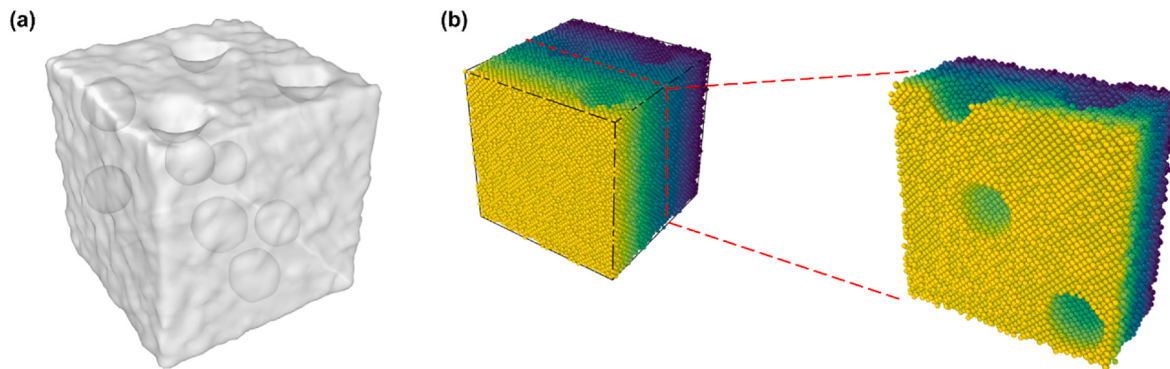


Fig. 2. MD visualization of the simulated nano porous HEA model S_a . (a) The defect mesh and (b) the simulation cell and a cross-sectional view showing the surface internal pore sites.

constructing foam structures utilizes the physical properties of the atoms to create spatial filters for generating pore sites [36,37]. However, it results in atoms isolated in the generated voids and presents challenges to multi-component systems. In the conventional modeling of metal foam structures, a sacrificial crystal structure is heated above its melting point to model a spatial filter. Due to equilibrium fluctuations, some atoms in the melt would have different temperatures. A cut-off temperature is set to remove atoms with temperatures above the set value, until a predetermined fill factor is achieved. Thereafter, all non-connected atoms and clusters are removed with a cluster detector [42]. The resulting structure—spatial filter—is used to remove all superfluous atoms from the nonporous crystalline metal.

This modeling approach is not applicable to HEAs because HEAs are composed of five or more primary elements. During heating, equilibrium fluctuations of the atoms in the melt would be more prominent in some elements than others. Hence, the application of a cut-off temperature would result in the non-uniform removal of atoms. The generated spatial filter would preferentially remove certain elements of the nonporous HEA system, altering its molar ratio. Thus, the foam structure would have a molar ratio different from the predefined molar ratio of the nonporous structure. Also, the use of spatial filters hinders the modeling of foam structures with specified pore locations. Although a spatial filter modeled from a single-element crystal structure can resolve the variation in molar ratio, atom removal remains random in this approach. Thus, modeling of HEA foams with predetermined pore locations is not feasible with the conventional technique, and as such its effect on the mechanical properties cannot be investigated.

To study the effect of porosity on mechanical behavior, the total volume of the created voids was varied from 5% to 30% at a 5% increment. Variation was achieved by evaluating the radius of each void by numerical calculations to obtain the required percent porosity. It is mathematically expressed as:

$$\%P = \frac{V_p}{V_T} \times 100\% \quad (1)$$

where $\%P$ is the percent porosity, V_p is the pore volume and V_T is the total volume.

Thereafter, uniaxial tensile deformation of the CoCrFeMnNi HEA foam structures was conducted at a strain rate of 0.001 ps^{-1} in the $<100>$ plane. Deformation was carried out on the modeled foam structures at the respective temperatures and a pressure of 0 bar in the $<010>$ and $<001>$ planes. The structure visualization and analysis were done using OVITO [43]. Also, the dislocation planes of the foam structures were extracted using the dislocation extraction algorithm (DXA) [44].

Herein, the calculated stress is the Virial Stress. It is a derivative of the Clausius Virial Theorem and the Maxwell velocity distribution [45]. The Viral stress is calculated using the equation below.

$$\sigma_{ij} = \frac{1}{V} \sum_{\alpha} \left[\frac{1}{2} \sum_{\beta=1}^N (r_i^{\beta} - r_i^{\alpha}) F_j^{\alpha\beta} + m^{\alpha} v_i^{\alpha} v_j^{\alpha} \right] \quad (2)$$

where σ_{ij} calculates the stress experienced by an atom α owing to neighboring atoms β ($\beta = 1$ to N), V is the volume of the system, i and j represent x, y and z direction, v_i^{α} and v_j^{α} are velocities of atom α in the direction i and j , m^{α} is the mass of atom α , r_i^{α} and r_i^{β} are the position of atom α and β in direction i , and $F_j^{\alpha\beta}$ is the force experienced by atom α owing to atom β in direction j [46].

3. Results and discussion

3.1. Effect of atom distribution

The stress-strain curves and the effect of porosity on ultimate tensile strength for the simulated equiatomic CoCrFeMnNi HEA foam is shown in Fig. 3. At a constant temperature of 300 K, all three distinct arrangements of atoms display similar behavior (see Fig. S1). However, each percent porosity demonstrated unique yield point values followed by stress drops. The plots of the ultimate tensile strength against percent porosity showed different UTS values at each percentage porosity. Thus, for all the atom distribution studied, the ultimate tensile strength decreased as the porosity percentage increased. The uniform distribution of the atoms suggests that there is an equal amount of reduction of each element in the porous structure, consequently, the mechanical behavior of the equiatomic CoCrFeMnNi HEA foam is independent of the atom distribution.

From the obtained stress-strain curves, it is observed that the tensile stress increases linearly with an increase in strain at low strain values ($\epsilon < 0.02$). In response to higher strain values ($\epsilon > 0.02$), a nonlinear behavior of the stress was observed. Such response has been reported as elastic softening [47]. The observed elastic softening of the simulated HEAs resulted from a decrease in the interatomic force gradient under tension. At the equilibrium interatomic spacing, thus the first neighbor spacing of two atoms, atoms of a lattice are in equilibrium positions and have the lowest energies. Subsequently, the tensile strain applied to the lattice increases the cohesive energy and interatomic separation which generates extra stress within the structure due to the attraction between the atoms. Table 1 summarizes the average UTS and elastic modulus of the simulated CoCrFeMnNi HEA foams of different atom distributions. As porosity increased, both the UTS and elastic modulus decreased. As compared to a nonporous CoCrFeMnNi HEA, the pores of the foam structure act as stress concentrators. For an isolated spherical pore, the applied tensile stress is amplified by a factor of 2 [48]. Hence, the tensile strength and stiffness of the foam structure declines as porosity increases.

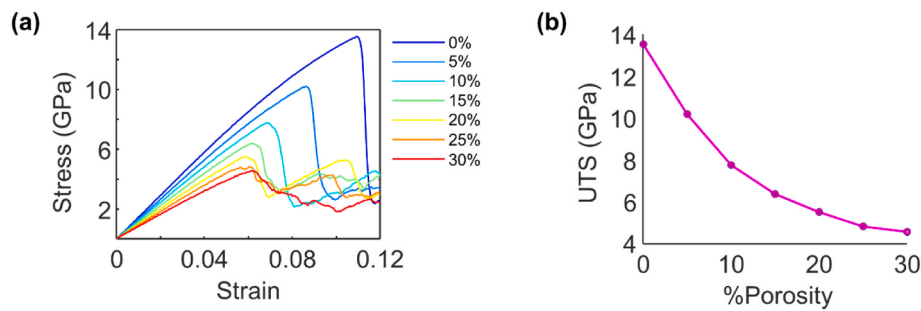


Fig. 3. Mechanical behavior of CoCrFeMnNi HEA foam under uniaxial tensile deformation at ambient temperature (300 K). (a) Engineering stress-strain curves for the simulated HEA atom distribution, model S_a , at various percent porosity and (b) the effect of porosity on ultimate tensile strength.

Table 1

Average Ultimate Tensile Strength (UTS) and Elastic Modulus (E_m) of CoCrFeMnNi HEA foams.

%Porosity	0%	5%	10%	15%	20%	25%	30%
UTS(GPa)	13.5118	10.0846	7.8667	6.4366	5.5074	4.8489	4.5515
E_m (GPa)	144.7433	133.1279	122.7811	111.9852	101.6024	92.5528	83.2759

3.2. Effect of temperature

The temperature effect on mechanical properties of the CoCrFeMnNi HEA foam is shown in Fig. 4. Similar deformation behavior was observed for all the modeled HEA systems at different temperatures and atom distributions (see Fig. S2 and Fig. S3). A three-stage phenomenon was noted. In stage I, a linear rise in tensile strength is observed i.e., at lower strains ($\epsilon < 0.02$). A nonlinear increase in stress with strain at higher strain values was recorded in stage II which was followed by a final sharp stress drop in stage III. The three stages correspond to elasticity, plasticity, and fracture, respectively. The Hooke's law governs the observed linear increase and hence the elastic modulus of the alloy can be determined by linear fitting of the slope in this stage. The nonlinear response reflects the permanent deformation of the alloy, and the observed sharp drop in the stress-strain curve indicates fracture. The findings in the present study indicate that the mechanical properties of both the nonporous CoCrFeMnNi HEA and HEA CoCrFeMnNi HEA

foams are sensitive to temperature.

For both structures, the ultimate tensile strength and elastic modulus increased as the temperature decreased. In comparison to the lattice of the CoCrFeMnNi HEA at lower temperatures, the high entropy associated with elevated temperatures leads to a significant increase in the amplitude of atomic vibrations. The intensity of thermal atomic motion increases and the bonding energy between atoms decreases. This is demonstrated in the mean square displacement (MSD) and the radial distribution function (RDF) plots at different temperatures shown in Fig. 5. MSD measures the average distance moved by particles or deviation of particles from their initial position in the lattice over time. It can be observed that the computed MSD values of the system increase with rise in temperature. The height of a peak in an RDF plot corresponds to the probability of finding atoms at a specific interatomic distance. It can be observed that the height of the peaks reduces as temperature increases from 77 K to 1000 K.

As temperature increases, the atoms gain kinetic energy and start to

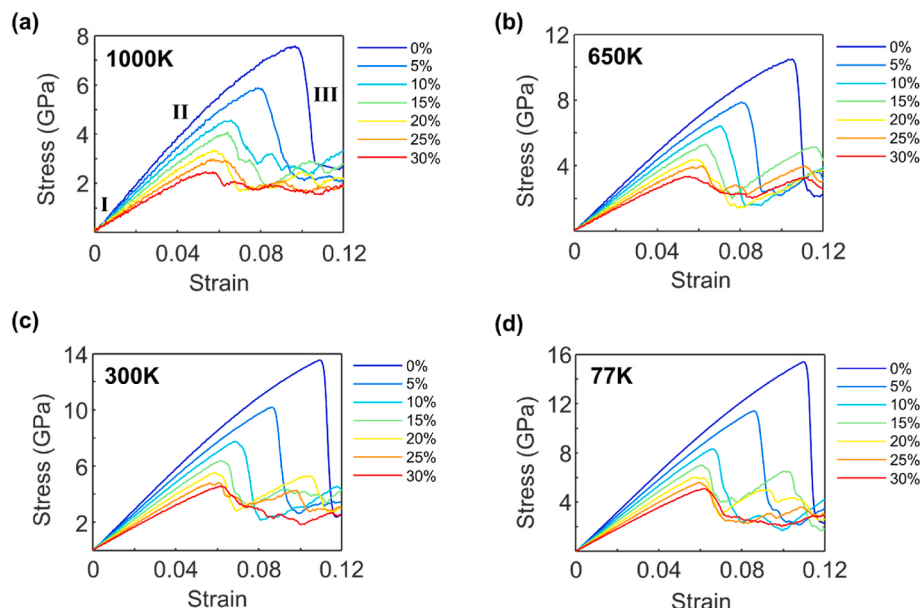


Fig. 4. Effect of temperature and porosity on the mechanical behavior of CoCrFeMnNi HEA foam under uniaxial tensile deformation with atom distribution S_a . Engineering stress-strain curves for the simulated HEA models at various percent porosity and temperatures; (a) 1000 K (b) 650 K, (c) 300 K, and (d) 77 K. The three-stage phenomenon (I, II and III), describing the mechanical behavior, is illustrated in plot (a).

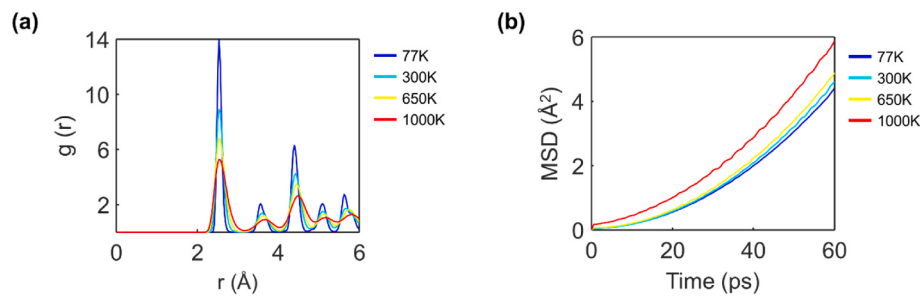


Fig. 5. Effect of temperature on atomic movements in CoCrFeMnNi HEA foam with atom distribution S_a and 15% percent porosity. Plots of (a) radial distribution function against pair separation distance and (b) mean square displacement against time, at the simulated temperatures.

vibrate more rapidly leading to increased MSD values. The resulting thermal atomic motion causes the atoms to occupy a larger volume, and the interatomic distance between the nearest neighbors increases. The probability of finding atoms at a given distance decreases as the interatomic distance increases. The height of the peaks in the RDF plots are consequently reduced. In addition, the bond energy between atoms generally decreases as interatomic distance increases. Thus, the thermal atomic motion also weakens the bonds between the atoms, which further decreases the height of the peaks. This is because the attractive force between atoms decreases with increasing distance, which leads to a decrease in potential energy. Subsequently, relatively lower peaks are observed at high temperatures due to the increased interatomic distance

and weakening of bonds between the atoms. As a result, atomic bonds easily break, and the HEA lattice becomes more susceptible to deformation at elevated temperatures which causes the reduction in both the UTS and elastic modulus. Considering the relation between temperature and the UTS of the CoCrFeMnNi HEA foams of different atom distributions and percent porosity, a reduction in UTS as temperature increased was observed for all percent porosities (see Fig. S4). This suggests that irrespective of the atomic distribution, the UTS of the HEA foam is inversely related to both porosity and temperature.

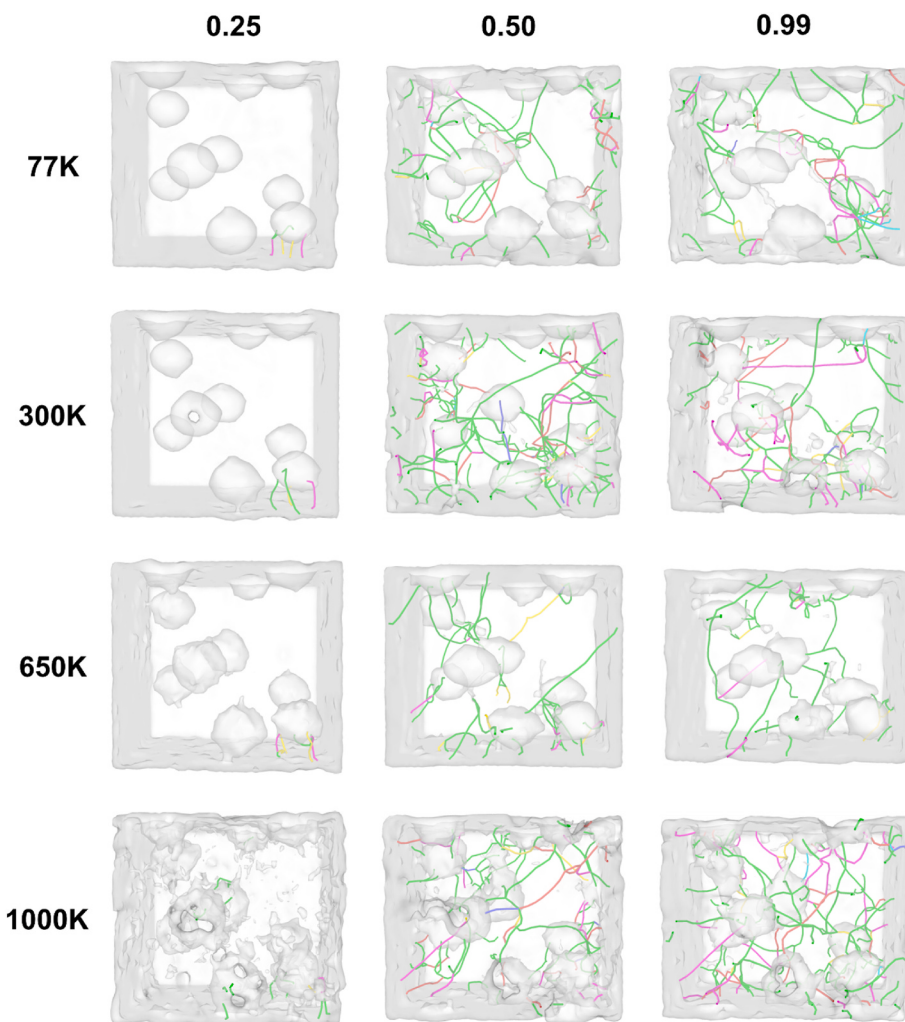


Fig. 6. Dislocation distributions in CoCrFeMnNi HEA foam under uniaxial tensile loading at low porosity (5%). Simulation snapshots of the defect mesh at 0.25, 0.50 and 0.99 (before fracture) fractions of the applied strain for the simulated temperatures of 77 K, 300 K, 650 K, and 1000 K. The corresponding dislocations are represented by lines; $\frac{1}{2} \langle 110 \rangle$ Perfect (blue), $\frac{1}{6} \langle 112 \rangle$ Shockley partials (green), $\frac{1}{6} \langle 110 \rangle$ Stair-rod partials (pink), $\frac{1}{3} \langle 111 \rangle$ Frank partials (cyan), and $\frac{1}{3} \langle 100 \rangle$ Hirth partials (yellow). (For interpretation of the references to colour in this figure legend, the reader is referred to the Web version of this article.)

3.3. Deformation mechanism

The defect mesh of the CoCrFeMnNi HEA foam structures at different temperatures and strains is shown in Fig. 6 for a low percent porosity and in Fig. 7 for a high percent porosity. As temperature increases dislocations emerge at low strain rates, due to the ease of deformation at high temperatures. More dislocations are generated at low percent porosity with longer dislocation lengths and fewer crack propagations. On the other hand, less dislocations are generated at high percent porosity with shorter dislocation lengths and more crack propagations. However, the distribution of dislocations within the structure varies with both strain and temperature due to void nucleation and crack propagation. Also, the impact of temperature on the peak stress and flow stress of materials causes the disparity between the frequency of dislocation slippage and the formation of deformation twins [49].

Under uniaxial tensile stress, the structure undergoes elastic deformation where the lattice is strained without the formation of dislocations. Further, it undergoes plastic deformation where atoms move from equilibrium lattice positions leading to dislocations, thus an instantaneous change in atomic arrangements of the lattice. As shown in the defect mesh, both partial and perfect dislocations were generated in the CoCrFeMnNi HEA foam structures as the strain increased. Due to the intense localized stress created by the pores under loading, the realized dislocations emerge from the pore sites. The generated partial dislocations in the structure include Shockley partials, Stair-rod partials, Frank partials, and Hirth partials. For all the percent porosities of the modeled HEA foam, the Shockley partials were the most partial dislocations

observed (refer to Supplementary material).

The strained crystal structure undergoes dislocation movements which increase the dislocation density during tensile deformation. Under deformation, high dislocation density of the HEA foam structure is observed at low percent porosity causing high intensities of dislocation intersection. Contrarily, the intensity of dislocation intersection diminishes as the percent porosity increases. The inter-pore distance is relatively short at high percent porosity (see Fig. 7, Fig. S7 and Fig. S8). Subsequently, the movement of dislocation from one pore site to the other is easily achieved, and dislocations easily result in void nucleation. Hence, there is less accumulation of dislocations to form intersects, thus, low dislocation density at high percent porosity. Also, the dislocation density of the alloy varies with temperature during deformation. A rise in temperature expands the cell, consequently decreasing the dislocation density [50]. Thus, the dislocation density considerably declines as temperature increases. Intensified dislocation intersects hinder plastic deformation and increases deformation resistance. As a result, the tensile strength and elastic modulus of the alloy decreases at low dislocation density. In addition, the resulting thermal activation energy due to temperature enhances dislocation by overcoming short-range energy barriers [38], and hence the tensile strength and elastic modulus of the alloy decreases (see Fig. S4).

Here, we focus on the Shockley partial dislocation as it is the predominant partial dislocation observed, a major contributor to the dislocation density of the structure, and the leading cause of stacking faults in crystal structures. The propagation of $1/6\langle 211 \rangle$ Shockley partial dislocations in the lattice forms the observed intrinsic stacking

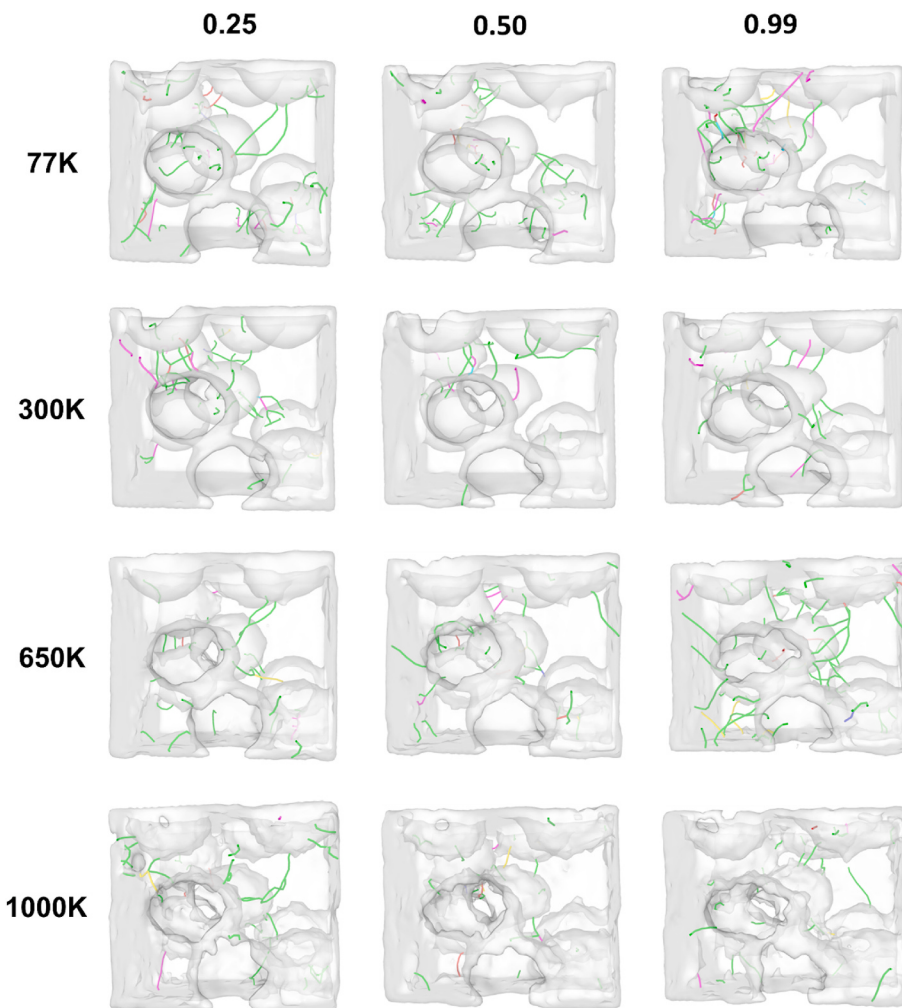


Fig. 7. Dislocation distributions in CoCrFeMnNi HEA foam under uniaxial tensile loading at high porosity (30%). Simulation snapshots of the defect mesh at 0.25, 0.50 and 0.99 (before fracture) fractions of the applied strain for the simulated temperatures of 77 K, 300 K, 650 K, and 1000 K. The corresponding dislocations are represented by lines; $\frac{1}{2} \langle 110 \rangle$ Perfect (blue), $\frac{1}{6} \langle 112 \rangle$ Shockley partials (green), $\frac{1}{6} \langle 110 \rangle$ Stair-rod partials (pink), $\frac{1}{3} \langle 111 \rangle$ Frank partials (cyan), and $\frac{1}{3} \langle 100 \rangle$ Hirth partials (yellow). (For interpretation of the references to colour in this figure legend, the reader is referred to the Web version of this article.)

faults in the crystal structure. Intrinsic stacking faults give rise to extrinsic stacking faults and deformation twins. Intrinsic stacking faults convert the ABCABC stacking sequence of FCC to an HCP stacking sequence as illustrated in Fig. 8. The B layer after the A layer in the FCC stacking sequence becomes a C layer resulting in an HCP stacking sequence. Another Shockley partial dislocation propagates on the parallel slip plane leading to extrinsic stacking faults. Subsequently, the formed ABCAC stacking sequence becomes ABCBA characterizing the deformation twins [33]. Thus, the propagation of Shockley partial dislocations on neighboring planes of existing extrinsic stacking faults creates deformation twins. In comparison, the nucleation of deformation twins in nonporous HEA is homogeneous due to the propagation of Shockley partial dislocations on adjacent planes $\langle 111 \rangle$ whereas the nucleation in the porous HEA is restricted to the pore sites.

The generated stacking faults within the structure intersect upon further straining and forms vacancy strings resulting in void nucleation [51]. Emitting dislocations transform vacancy strings perpendicular to the loading axis transforms into voids leading to crack initiation and propagation from the pore sites. It can be observed that pores are the crack initiation sites in the deformation of the CoCrFeMnNi HEA foam structure. Pores are defects in the crystal structure and act as stress concentrators. Due to the stress fields surrounding the pores, dislocations, stacking faults and deformation twins propagate from one pore site to the other leading to cracks. Consequently, the stress-bearing capacity of the foam decreases and causes a significant reduction in the ultimate tensile Strength and elastic modulus.

3.4. Effect of pore location

To further investigate the factors that influence the mechanical properties of the CoCrFeMnNi HEA foam, the location of the generated pores was varied and tested under uniaxial tension at 300 K. Here, two additional HEA foam models were developed with atom distribution S_a . One system, model S_{ac} , was modeled with all the pore sites located within the structure at 10 Å from the edges of the simulation cell while the other system, model S_{as} , had the pore sites perpendicularly toward the exterior of the simulation cell such that the pores were on the surface of the structure. Fig. 9 compares the stress-strain curve of the new structures, models S_{ac} and S_{as} with closed pores and surface pores, respectively, to the previous hybrid structure, model S_{ah} which had both closed and surface pores.

Irrespective of the pore location, it was observed that an increase in percent porosity resulted in a decline in the ultimate tensile strength of all the simulated systems. In comparing the systems modeled, the structure with closed pores results in the highest decrease in UTS while

surface pore structures showed the least decline in UTS. Interestingly, a hybrid structure does not lead to enhanced properties. The hybrid structure showed a lesser UTS as compared to the surface pore structure. Due to the applied stress on the material, cracks initiate and propagate within the structure causing failure, hence the total stress the material can withstand before failure is reduced. Comparably, the closed pores are more detrimental to mechanical properties since they are located within the structure. A minimal difference in UTS was observed among the structures at 5% porosity while a distinctive UTS change was observed at 10% porosity, particularly for the surface pore structure. Using the hybrid model as a reference, the UTS of the surface pore structure increased from 8% at 5% porosity to 20% at 10% porosity. The superior mechanical behavior of the structure with surface pores at high percent porosity is attributed to the crack propagation distance. The crack propagation distance between pores decreases as the percent porosity increases. Hence, at higher percent porosity, the structures with closed pores are unable to withstand high tensile stress before failure. Thus, they are more susceptible to deformation.

4. Conclusion

High entropy alloys possess good mechanical properties and demonstrate great potential for various engineering applications. Atomistic simulations have greatly aided in understanding and predicting the behavior of HEAs under different conditions. In this study, molecular dynamics simulation was used to model an equiatomic nano porous CoCrFeMnNi HEA as a foam structure and to understand the structure-property relationship. The change in mechanical properties of the HEA foam in terms of atom distribution, percent porosity, and temperature was investigated. The results indicated similar mechanical properties of the HEA samples among the three different atom distributions. On the other hand, an increase in the percent porosity and temperature resulted in a decrease in the ultimate tensile strength and the elastic modulus of the HEA foam. The ultimate tensile strength consistently decreased from 15.51 GPa at 0% porosity to 4.55 GPa at 30%.

The deformation mechanism of the foam structures at different temperatures and percent porosity was also investigated. The initial plastic deformation depends on dislocation slippage and dislocations emerge from the pores. Under the direction of leading Shockley partial dislocations, intrinsic stacking faults move across the entire lattice. The primary plastic deformation mode is the occurrence of intrinsic stacking faults due to dislocation slippage. The interactions among intrinsic stacking faults induce FCC to HCP phase transformations, consequently, deformation twins are observed in the phase transformation regions.

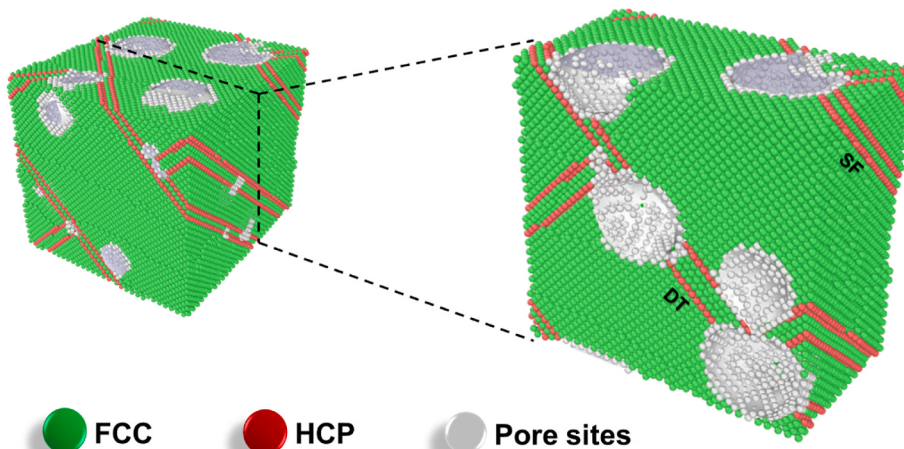


Fig. 8. Deformation of CoCrFeMnNi HEA foam under uniaxial tensile loading at ambient temperature (300 K). The simulated HEA foams demonstrate Stacking Faults (SF) and Deformation Twins (DT).

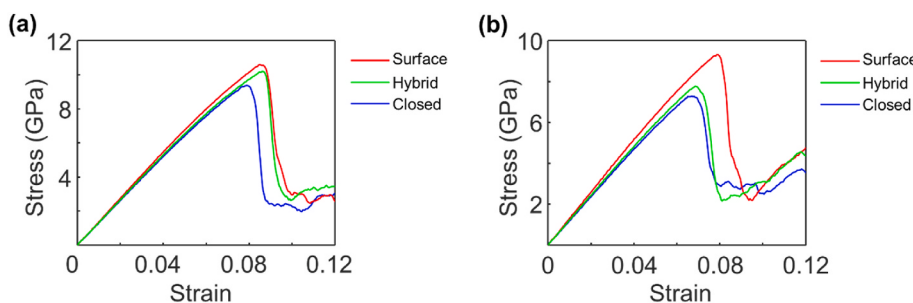


Fig. 9. Effect of pore location on the mechanical behavior of CoCrFeMnNi HEA foam under uniaxial tensile deformation with atom distribution S_a , at a temperature of 300 K; (a) 5% porosity and (b) 10% porosity.

After establishing the relationship between the mechanical behavior of the HEA foam and the variations above, thus, atom distribution, percent porosity, and temperature, the location of the pore sites were altered to determine which collective pore locations improve the UTS. Comparably, surface pores caused the least decline in UTS. The results presented here provide guidance to material design for the fabrication of HEA foams with high performance and an understanding of its failure mechanism under loading.

Credit authors statement

Ezekiel Edward Nettey-Oppong: Methodology, Writing original draft, Visualization, Formal analysis, Conceptualization, Investigation. **Emmanuel Essel Mensah:** Writing - original draft, Formal analysis, Investigation. **Elijah Effah:** Writing original draft, Investigation. **Eric Asare:** Supervision, Validation, Writing - review & editing. **Martinson Addo Nartey:** Supervision, Validation, Formal analysis, Investigation, Writing - review & editing.

Declaration of competing interest

The authors declare that they have no known competing financial interests or personal relationships that could have appeared to influence the work reported in this paper.

Data availability

I have shared the link to my research data at the Attach File step

Appendix A. Supplementary data

Supplementary data to this article can be found online at <https://doi.org/10.1016/j.ssc.2023.115236>.

References

- [1] M. Abada, A. Ibrahim, Hybrid multi-cell thin-walled tubes for energy absorption applications: blast shielding and crashworthiness, Compos. B Eng. 183 (2020), 107720.
- [2] A. Nazir, S.-C. Lin, J.-Y. Jeng, Parametric investigation of functionally gradient wave springs designed for additive manufacturing, Int. J. Adv. Des. Manuf. Technol. 119 (2022) 1673–1691.
- [3] J. Zhang, G. Lu, Z. You, Large deformation and energy absorption of additively manufactured auxetic materials and structures: a review, Compos. B Eng. 201 (2020), 108340.
- [4] O. Rahman, K.Z. Uddin, J. Muthulingam, G. Youssef, C. Shen, B. Koohbor, Density-Graded cellular solids: mechanics, fabrication, and applications, Adv. Eng. Mater. 24 (2022), 2100646.
- [5] M. Salehi, S.M.H. Mirbagheri, A.J. Ramiani, Efficient energy absorption of functionally-graded metallic foam-filled tubes under impact loading, Trans. Nonferrous Metals Soc. China 31 (2021) 92–110.
- [6] G. Sun, D. Chen, G. Zhu, Q. Li, Lightweight hybrid materials and structures for energy absorption: a state-of-the-art review and outlook, Thin-Walled Struct. 172 (2022), 108760.
- [7] G. Youssef, N. Reed, N.U. Huynh, B. Rosenow, K. Manlulu, Experimentally-validated predictions of impact response of polyurea foams using viscoelasticity based on bulk properties, Mech. Mater. 148 (2020), 103432.
- [8] J. Meng, T.-W. Liu, H.-Y. Wang, L.-H. Dai, Ultra-high energy absorption high-entropy alloy syntactic foam, Compos. B Eng. 207 (2021), 108563.
- [9] A.D. Akinwekomi, C.-Y. Tang, G.C.-P. Tsui, W.-C. Law, L. Chen, X.-S. Yang, M. Hamdi, Synthesis and characterisation of floatable magnesium alloy syntactic foams with hybridised cell morphology, Mater. Des. 160 (2018) 591–600.
- [10] G. Anbucchezhiyan, T. Muthuramalingam, B. Mohan, Effect of process parameters on mechanical properties of hollow glass microsphere reinforced magnesium alloy syntactic foams under vacuum die casting, Arch. Civ. Mech. Eng. 18 (2018) 1645–1650.
- [11] D.W. Rao, Y.W. Yang, Y. Huang, J.B. Sun, L.W. Pan, Z.L. Hu, Microstructure and compressive properties of aluminum matrix syntactic foams containing Al2O3 hollow particles, Kovove Materialy-Metallic Mater. 58 (2020) 395–407.
- [12] A. Szlancsik, I.N. Orbulov, Compressive properties of metal matrix syntactic foams in uni-and triaxial compression, Mater. Sci. Eng. 827 (2021), 142081.
- [13] N. Movahedi, G.E. Murch, I. v Belova, T. Fiedler, Effect of heat treatment on the compressive behavior of zinc alloy ZA27 syntactic foam, Materials 12 (2019) 792.
- [14] L. Pan, Y. Yang, M.U. Ahsan, D.D. Luong, N. Gupta, A. Kumar, P.K. Rohatgi, Zn-matrix syntactic foams: effect of heat treatment on microstructure and compressive properties, Mater. Sci. Eng., A 731 (2018) 413–422.
- [15] Q. Yang, J. Cheng, Y. Wei, B. Yu, Z. Miao, P. Gao, Innovative compound casting technology and mechanical properties of steel matrix syntactic foams, J. Alloys Compd. 853 (2021), 156572.
- [16] C. Xie, H. Li, B. Yuan, Y. Gao, Z. Luo, M. Zhu, Ti3Sn-NiTi syntactic foams with extremely high specific strength and damping capacity fabricated by pressure melt infiltration, ACS Appl. Mater. Interfaces 11 (2019) 28043–28051.
- [17] Q. Halim, N.A.N. Mohamed, M.R.M. Rejab, W.N.W.A. Naim, Q. Ma, Metallic glass properties, processing method and development perspective: a review, Int. J. Adv. Des. Manuf. Technol. 112 (2021) 1231–1258.
- [18] X. Chen, W. Xie, J. Zhu, Z. Wang, Y. Wang, Y. Ma, M. Yang, W. Jiang, H. Yu, Y. Wu, Influences of Ti additions on the microstructure and tensile properties of AlCoCrFeNi2. 1 eutectic high entropy alloy, Intermetallics (Barking). 128 (2021), 107024.
- [19] F. He, Z. Yang, S. Liu, D. Chen, W. Lin, T. Yang, D. Wei, Z. Wang, J. Wang, J. Kai, Strain partitioning enables excellent tensile ductility in precipitated heterogeneous high-entropy alloys with gigapascal yield strength, Int. J. Plast. 144 (2021), 103022.
- [20] Y. Tong, D. Chen, B. Han, J. Wang, R. Feng, T. Yang, C. Zhao, Y.L. Zhao, W. Guo, Y. Shimizu, Outstanding tensile properties of a precipitation-strengthened FeCoNiCrTiO. 2 high-entropy alloy at room and cryogenic temperatures, Acta Mater. 165 (2019) 228–240.
- [21] Y. Wu, X. Zhao, Q. Chen, C. Yang, M. Jiang, C. Liu, Z. Jia, Z. Chen, T. Yang, Z. Liu, Strengthening and fracture mechanisms of a precipitation hardening high-entropy alloy fabricated by selective laser melting, Virtual Phys. Prototyp. 17 (2022) 451–467.
- [22] T. Zheng, X. Hu, F. He, Q. Wu, B. Han, D. Chen, J. Li, Z. Wang, J. Wang, J. Kai, Tailoring nanoprecipitates for ultra-strong high-entropy alloys via machine learning and prestrain aging, J. Mater. Sci. Technol. 69 (2021) 156–167.
- [23] Y. Lu, X. Gao, L. Jiang, Z. Chen, T. Wang, J. Jie, H. Kang, Y. Zhang, S. Guo, H. Ruan, Y. Zhao, Z. Cao, T. Li, Directly cast bulk eutectic and near-eutectic high entropy alloys with balanced strength and ductility in wide temperature range, Acta Mater. 124 (2017) 143–150, <https://doi.org/10.1016/j.actamat.2016.11.016>.
- [24] S. Gorsse, F. Tancret, Current and emerging practices of CALPHAD toward the development of high entropy alloys and complex concentrated alloys, J. Mater. Res. 33 (2018) 2899–2923.
- [25] C. Lee, G. Song, M.C. Gao, R. Feng, P. Chen, J. Brechtl, Y. Chen, K. An, W. Guo, J. D. Poplawsky, Lattice distortion in a strong and ductile refractory high-entropy alloy, Acta Mater. 160 (2018) 158–172.
- [26] A.S. Sharma, S. Yadav, K. Biswas, B. Basu, High-entropy alloys and metallic nanocomposites: processing challenges, microstructure development and property enhancement, Mater. Sci. Eng. R Rep. 131 (2018) 1–42.
- [27] Y. Yin, Development of Cost-Effective High-Entropy Alloys with Superior Mechanical Properties, 2021.

- [28] J. Meng, Y. Qiao, T.-W. Liu, Y.-Y. Tan, F.-H. Cao, Y. Chen, H.-Y. Wang, L.-H. Dai, Eutectic high entropy alloy syntactic foam, *J. Mater. Sci. Technol.* 149 (2023) 177–189, <https://doi.org/10.1016/j.jmst.2022.12.009>.
- [29] J. Yeh, S. Chen, S. Lin, J. Gan, T. Chin, T. Shun, C. Tsau, S. Chang, Nanostructured high-entropy alloys with multiple principal elements: novel alloy design concepts and outcomes, *Adv. Eng. Mater.* 6 (2004) 299–303.
- [30] C.-J. Tong, Y.-L. Chen, J.-W. Yeh, S.-J. Lin, S.-K. Chen, T.-T. Shun, C.-H. Tsau, S.-Y. Chang, Microstructure characterization of Al x CoCrCuFeNi high-entropy alloy system with multiprincipal elements, *Metall. Mater. Trans.* 36 (2005) 881–893.
- [31] F. Otto, A. Dlouhý, Ch Somsen, H. Bei, G. Eggeler, E.P. George, The influences of temperature and microstructure on the tensile properties of a CoCrFeMnNi high-entropy alloy, *Acta Mater.* 61 (2013) 5743–5755, <https://doi.org/10.1016/j.actamat.2013.06.018>.
- [32] W. Li, H. Fan, J. Tang, Q. Wang, X. Zhang, J.A. El-Awady, Effects of alloying on deformation twinning in high entropy alloys, *Mater. Sci. Eng.* 763 (2019), 138143.
- [33] J. Liu, Molecular dynamic study of temperature dependence of mechanical properties and plastic inception of CoCrFeNi high-entropy alloy, *Phys. Lett.* 384 (2020), 126516.
- [34] M. Meraj, S. Pal, Deformation of Ni20W20Cu20Fe20Mo20 high entropy alloy for tensile followed by compressive and compressive followed by tensile loading: a molecular dynamics simulation based study, in: IOP Conf Ser Mater Sci Eng, IOP Publishing, 2016, 12019.
- [35] A. Sharma, G. Balasubramanian, Dislocation dynamics in Al0.1CoCrFeNi high-entropy alloy under tensile loading, *Intermetallics (Barking)*. 91 (2017) 31–34.
- [36] N. Gunkelmann, Y. Rosandi, C.J. Ruestes, E.M. Bringa, H.M. Urbassek, Compaction and plasticity in nanofoams induced by shock waves: a molecular dynamics study, *Comput. Mater. Sci.* 119 (2016) 27–32, <https://doi.org/10.1016/j.commatsci.2016.03.035>.
- [37] N. Gunkelmann, E.M. Bringa, Y. Rosandi, Molecular dynamics simulations of aluminum foams under tension: influence of oxidation, *J. Phys. Chem. C* 122 (2018) 26243–26250.
- [38] Z.H. Sun, J. Zhang, G.X. Xin, L. Xie, L.C. Yang, Q. Peng, Tensile mechanical properties of CoCrFeNiTiAl high entropy alloy via molecular dynamics simulations, *Intermetallics (Barking)*. 142 (2022), 107444.
- [39] L. Li, H. Chen, Q. Fang, J. Li, F. Liu, Y. Liu, P.K. Liaw, Effects of temperature and strain rate on plastic deformation mechanisms of nanocrystalline high-entropy alloys, *Intermetallics (Barking)*. 120 (2020), 106741.
- [40] A.P. Thompson, H.M. Aktulg̃, R. Berger, D.S. Bolintineanu, W.M. Brown, P. Crozier, P.J. in't Veld, A. Kohlmeyer, S.G. Moore, T.D. Nguyen, LAMMPS—a flexible simulation tool for particle-based materials modeling at the atomic, meso, and continuum scales, *Comput. Phys. Commun.* 271 (2022), 108171.
- [41] R. Gröger, V. Vitek, A. Dlouhý, Effective pair potential for random fcc CoCrFeMnNi alloys, *Model. Simulat. Mater. Sci. Eng.* 28 (2020), 75006, <https://doi.org/10.1088/1361-651x/ab7f8b>.
- [42] S.D. Stoddard, Identifying clusters in computer experiments on systems of particles, *J. Comput. Phys.* 27 (1978) 291–293.
- [43] A. Stukowski, Visualization and analysis of atomistic simulation data with OVITO—the Open Visualization Tool, *Model. Simulat. Mater. Sci. Eng.* 18 (2009), 15012, <https://doi.org/10.1088/0965-0393/18/1/015012>.
- [44] A. Stukowski, K. Albe, Dislocation detection algorithm for atomistic simulations, *Model. Simulat. Mater. Sci. Eng.* 18 (2010), 25016, <https://doi.org/10.1088/0965-0393/18/2/025016>.
- [45] D.H. Tsai, The virial theorem and stress calculation in molecular dynamics, *J. Chem. Phys.* 70 (1979) 1375–1382.
- [46] A.K. Subramanyan, C.T. Sun, Continuum interpretation of virial stress in molecular simulations, *Int. J. Solid Struct.* 45 (2008) 4340–4346.
- [47] L. Zhang, C. Lu, A.K. Tieu, Nonlinear elastic response of single crystal Cu under uniaxial loading by molecular dynamics study, *Mater. Lett.* 227 (2018) 236–239.
- [48] W.D. Callister Jr., D.G. Rethwisch, Callister's Materials Science and Engineering, John Wiley & Sons, 2020.
- [49] Y. Qi, X. Chen, M. Feng, Molecular dynamics-based analysis of the effect of temperature and strain rate on deformation of nanocrystalline CoCrFeMnNi high-entropy alloy, *Appl. Phys. A* 126 (2020) 1–10.
- [50] M.R. Staker, D.L. Holt, The dislocation cell size and dislocation density in copper deformed at temperatures between 25 and 700°C, *Acta Metall.* 20 (1972) 569–579, [https://doi.org/10.1016/0001-6160\(72\)90012-0](https://doi.org/10.1016/0001-6160(72)90012-0).
- [51] W. W, P. Pang, G.-C. Zhang, A.-G. Zhang, X.-G. Xu, Zhao, Dislocation creation and void nucleation in FCC ductile metals under tensile loading: a general microscopic picture, *Sci. Rep.* 4 (2014) 6981, <https://doi.org/10.1038/srep06981>.